

Microstructures and Properties of Tantalum and Molybdenum Laser Welding for Electron Guns

Wang Bofeng^{1,2}, Hu Xuhua¹, Zhou Guanli¹, Zhou Jianyong¹, Zhang Yongqing¹,
Zhang Zhaochuan¹

¹ Key Laboratory of Science and Technology on High Power Microwave Sources and Technologies, Institute of Electronics, Chinese Academy of Sciences, Beijing 100190, China; ² University of Chinese Academy of Sciences, Beijing 100049, China

Abstract: Tantalum (Ta)/Molybdenum (Mo) dissimilar joint was successfully joined by laser welding process with pure Pt filler wire. The weld surface morphology, microstructure, interface element distribution, fracture morphology, phase structure, electrical performance and environment adaptability were studied by metallography microscope, scanning electron microscopy, hardness and electronic universal test machine, X-ray diffraction, electron micro-hardness and tensile test, vibration table and ultra-high high vacuum system. Laser parameters have profound effects on microstructures of the laser-welded joints. Pores were generated in the weld zone caused by the preferential vaporization of pure Pt filler metal. The weld zone mainly contained TaPt₂, TaPt₃ and MoPt phase, resulting in higher hardness in the weld zone than that of base metal. The joint fracture surface exhibited typical brittle fracture morphology. The electrical property and environment test examined the joints welding quality for electron guns. Meanwhile, the reliability of laser welding process in the development, production, and application of microwave tubes was verified.

Key words: tantalum; molybdenum; pure Pt filler wire; laser welding; microstructures; properties

Microwave tubes have been in development around the world for many years because of their important applications in radar, communication, television broadcast, electronic countermeasure, particle accelerator, plasma heating device, ITER (international thermonuclear experimental reactor) and other fields. Until today, microwave tubes still remain to be a hot spot in the field of vacuum electronic devices. Electron gun is the heart of microwave tubes, which plays a decisive role in the mechanical and electrical property of vacuum electron tubes^[1]. Many refractory metals are widely used in the electron gun due to special working environment, such as Ta and Mo with high melting points, small thermal expansion coefficient and good thermal conductivity. It is difficult to firmly connect these refractory metals by traditional resistance welding methods. Therefore, the fabrication technology is a great important

process for electron guns. It is well known that joining technology is one of the most important methods in materials processing. The successful joining of dissimilar metals are favorable for the broadening of their application fields. The joining technology of electron gun mainly includes resistance welding, argon-arc welding, brazing, electron beam welding, and laser welding, and so on. With the rapid development of laser technology, laser welding is widely used for microwave tubes, which belongs to special welding and thus plays an irreplaceable role. Nd:YAG pulsed laser welding is widely used to interconnect small refractory metals because of its advantages such as short welding cycle, and high accuracy of energy input.

There have been some research activities on the joining refractory metals^[2-6]. However, it is a great challenge to achieve the joining of Ta to Mo for their limited weldability.

Received date: May 05, 2019

Foundation item: National Natural Science Foundation of China (61771454)

Corresponding author: Zhang Zhaochuan, Ph. D., Professor, Institute of Electronics, Chinese Academy of Sciences, Beijing 100190, P. R. China, Tel: 0086-10-56535256, E-mail: zczhang@mail.ie.ac.cn

Copyright © 2020, Northwest Institute for Nonferrous Metal Research. Published by Science Press. All rights reserved.

Several studies were performed to understand and improve the weldability of refractory metals. Mo and its alloys exhibit poor mechanical properties of fusion welding, due to impurities and grain coarsening^[3,4]. On the other hand, Ta/Ta or other alloys joints is easier to be welded. Successful joining of titanium with tantalum by resistance welding^[7], diffusion bonding^[8,9] and laser welding^[10] was reported.

To our knowledge, few studies have focused on the welding method and processing technology of the Ta/Mo joint. According to Zhou et al.^[2], the cracking mechanism in Ta/Mo joint was that low ductility feature in fusion zone most certainly played a role in the transgranular propagation of cracking in the Ta/Mo joint. However, the weld joint was not effective connection for engineering application. In this work, laser welding of Ta/Mo dissimilar metal was comprehensively studied with pure Platinum (Pt) filler metal. The characteristic and regularity of welding were researched from the welding process and method. The laser welding reliability of joints were also verified by the application in electron guns and microwave tubes.

1 Experiment

The base metal used in this study was Ta and Mo with specimen dimensions of $\phi 26$ mm \times 0.5 mm \times 2.7 mm and $\phi 26.3$ mm \times 0.15 mm \times 2.5 mm, respectively. The chemical composition and the physical properties of the material used in pulsed laser welding process are shown in Table 1 and Table 2, respectively. Fig.1 shows the schematic illustration of laser welding process. Ta and Mo are refractory metals, with obvious distinctions, such as melting point, density, heat conductivity and specific heat capacity. The melting point of Mo is lower than that of Ta, while the thermal conductivity of Mo is three times higher than that of Ta. Ta is on the top and heat can be transmitted to Mo

directly. Ta and Mo are heated and melted at the same time; therefore, lap joint is designed in this work. The filler wire is platinum (pure Pt) with diameter of 0.3 mm, used as a transition metal.

A model SL-1GX-600 pulsed laser with maximum average power of 600 W was used for laser welding. The pulsed Nd:YAG laser used has 1064 nm wavelength with Xenon lamp. The focal length (distance) of 120 mm and laser spot size of 0.5 mm can be obtained on the surface. Pulsed laser was able to produce pulses with 0.1~20 ms duration and frequency range of 1~300 Hz. Pure argon gas with a coaxial nozzle at 10 L/min flow rate was used for gas shielding.

Surface preparation and high temperature vacuum annealing prior to welding is mandatory for Ta and Mo; therefore, in these experiments the samples were brushed mechanically with a stainless-steel brush and were cleaned by acetone and alcohol just prior to welding. Laser welding process was performed in bead on plate condition with no restraints on plates.

Samples were ground and polished according to standard metallographic methods and then etched with HF and HNO₃. An optical microscopy (Leica DM4000-5000B, Ernst-Leitz-Straße, D-35578 Wetzlar, Germany) was used to observe the micromorphology of the joint. The interface elemental diffusion analysis was performed using a scanning electron microscope (ZEISS EVO18, Carl Zeiss Co., Ltd, Germany). The amounts of metal elements were measured using energy dispersive spectroscopy (EDS) analysis. A Rigaku SmartLab Micro X-ray diffract meter (micro-XRD) was used to as a means of identifying the phases in the joint with a beam size of 0.4 mm. The micro hardness distribution was analyzed by microhardness tester (VMH-002VD, Walter Uhl techn. Mikroskopie GmbH & Co.KG, Asslar, Germany) and under 100 g load. The tensile strength of joints was tested by an electronic universal

Table 1 Chemical composition of the base metal Ta and Mo (wt%)

Ta	Fe	Si	Ni	W	Mo	Ti	Nb	O	C	H	N	Ta
	0.005	0.005	0.002	0.01	0.01	0.002	0.05	0.01	0.01	0.0015	0.0005	Bal.
Mo	O	N	C	Fe	Al	Si	Ni	W	Ca	Mg	-	Mo
	0.02	0.003	0.01	0.0015	0.005	0.006	0.005	0.3	0.002	0.003	-	Bal.

testing machine (HY-1080, Shanghai Heng Wing Precision Instrument Co. Ltd, Shanghai, China) at room temperature, and the loading speed is 1 mm/min. Random vibration and shock (DC-600-6, Suzhou Sushi Testing Group Co., Ltd, Suzhou, China) experiments were used to test the firmness of the welding joint. Electrical properties (DZQ200*500-01-A0, Beijing Naura Vacuum Technology Co., Ltd, Beijing, China) were measured by the high vacuum system.

Table 2 Thermophysical properties of materials used in this study

Property	Ta	Mo	Pt
Melting point/ $^{\circ}$ C	2996	2620	1772
Density/ $g\cdot cm^{-3}$	16.6	10.2	21.5
Thermal conductivity/ $W\cdot m^{-1}\cdot K^{-1}$	54.5	138	74.1
Specific heat/ $J\cdot kg^{-1}\cdot K^{-1}$	156.5	265.2	135
Coefficient of thermal expansion/ $\times 10^{-6} K^{-1}$	6.5	4.9	9.1
Absorption coefficient/%	0.18	0.4	0.11

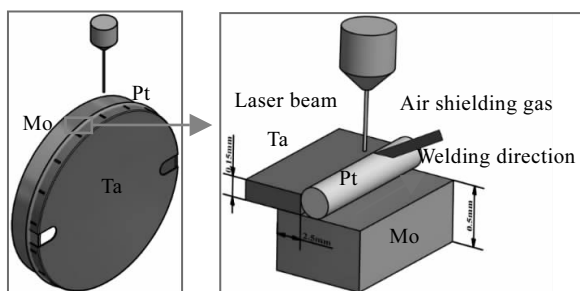


Fig.1 Schematic illustration of laser welding process

2 Results

2.1 Microstructures of laser-welded joints

The welding parameters have important influence on laser welding. The parameter optimization for pulsed Nd:YAG laser welding of Mo and Ta was comprehensively studied. The relation among the laser welding parameters, the cracking and blowholes was appropriately evaluated. The weld appearance is one of the most important factors when evaluating welding quality. Fig.2 show the weld surface morphologies of Ta/Mo joint with Pt filler metal. The molten pools of lap joints were of typical ladder shape characteristic. No cracks, pores and splash were found in the weld part. The experimental result indicated that the laser-welded joints consist of weld zone (WZ), heat affected zone (HAZ) and base metal (BM).

The parameter optimization for laser welding of Mo and Ta was comprehensively studied to obtain good quality of

joints. Fig.3 show the cross-sectional morphologies of Mo/Ta joint with Pt filler metal. With a 1100 W laser power, 4 ms pulse duration, +1 mm defocus distance, 3 Hz frequency and 10 L/min Argon shielding gas, crack/pore-free weld cross sections were achieved (as shown in Fig.3a). As the laser power decreases, pores appear (as shown in Fig.3b). Increasing the pulse duration has caused a reduction in weld width as can be seen in Fig.3c. According to Fig.3d, increasing the power to 1250 W has caused a reduction in the welding quality along with pores and cracks. When the power is 1100 W and pulse duration is 5 ms, Ta/Mo joint without filler metal is not formed successfully joined by laser conduction welding process with many small cracks. Zhou et al.^[2] showed similar phenomenon in the laser-welded joint of Ta and Mo. There is a severe cracking separated from the fuse zone mostly along weld centerline, and most of these cracks are transgranular with few cracks intergranular.

2.2 Cross section morphologies and phase structure

The optimized welding parameters are as follows: the output power is 1100 W, the pulse width is 4 ms, the pulse frequency is 3 Hz, the defocus distance is +1 mm and the Argon shielding gas is 10 L/min. With these welding technological parameters, cross-sectional morphologies and EDS analysis of the welding joint are shown in Fig.4 to obtain the concentration profiles of the alloying elements across the interface between the Pt weld zone and BM. Fig.4a and Fig.4b are cross-section of the Ta/Pt side in the joint and EDS line scanning analysis. It can be seen that few small hole defects exist in the WZ. Ta/Pt weld pool zone is between 8.5 and 12.5 μm with uniform width. Pt element enrichment occurred

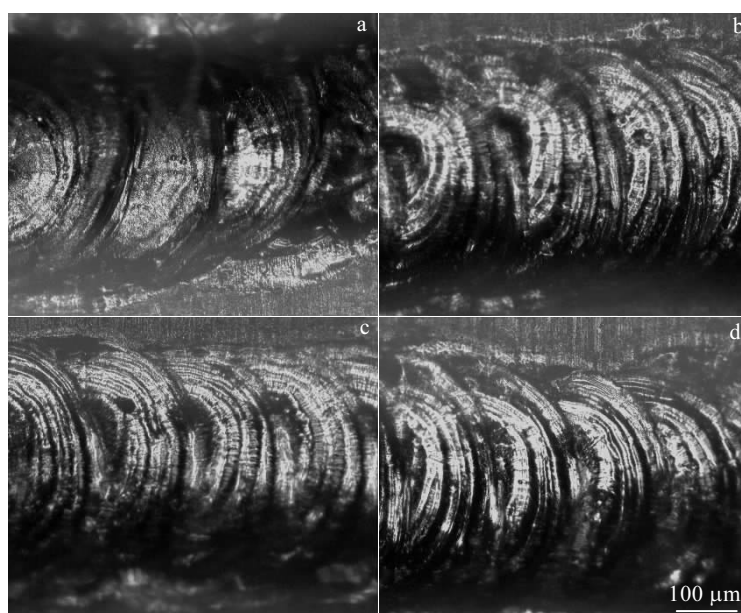


Fig.2 Weld surface morphologies of Mo/Ta joint with Pt: (a) $P=1018$ W, $\tau=4$ ms; (b) $P=1100$ W, $\tau=4$ ms; (c) $P=1100$ W, $\tau=5$ ms; (d) $P=1250$ W, $\tau=4$ ms

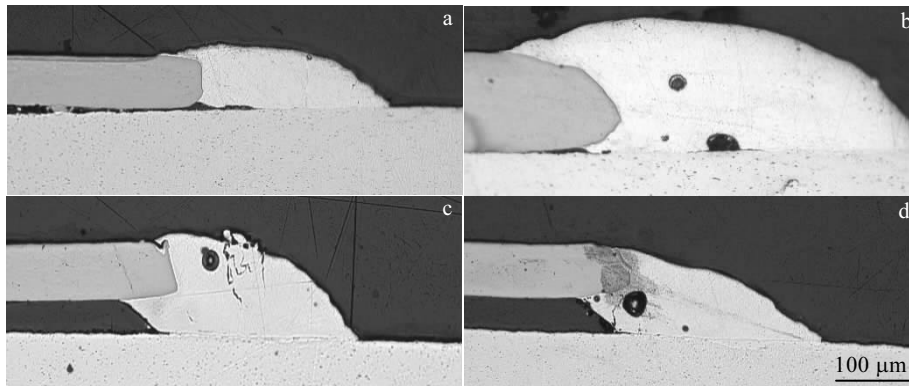


Fig.3 Microstructures of Mo/Ta joint with Pt: (a) $P=1100$ W, $\tau=4$ ms; (b) $P=1018$ W, $\tau=4$ ms; (c) $P=1100$ W, $\tau=5$ ms; (d) $P=1250$ W, $\tau=4$ ms

at the interface, indicating an occurrence of atomic diffusion or dissolution of the Pt element, which thereafter induced interfacial reaction. It caused formation of Ta–Pt reaction layers at the weld zone/Ta interface. Meanwhile, the Mo/Pt weld zone is narrow and thus, only few Mo and Pt elements have mutual diffusion (see Fig.4c and Fig.4d). Hence, metallurgical bonding was achieved at the Ta/Pt interface. It was similar to the observation reported by Zang et al.^[11]

To confirm the observation in Fig.4, micro-XRD analysis of the Ta /Mo joint is shown in Fig.5. It was found that Ta, Mo and Pt were the main phases, which were detected from the BM or filler metal. TaPt₂, TaPt₃, and MoPt phase formed at the interface, corresponding to reaction product of laser weld Ta and Mo using pure Pt filler metal. It indicated that TaPt₂ and TaPt₃ phase would

form in the case of joining solid Pt and a small amount of molten Ta, in accordance with the EDS analysis.

2.3 Mechanical property and fracture morphology

The shear strength of the Ta/Mo lap joints were measured for three samples in the same parameters. The average tensile strength was 50.2 MPa. The fracture location was in the weld zone of Mo/Pt interface. The fracture surface of the Ta/Mo joint (shown in Fig.6) clearly confirmed the cracking was transgranular, quasi-cleavage morphology with periodic steps, due to the overlapping individual spot welds of pulsed heat source. The grains coarsened in the weld zone were the main reason of the brittle fracture of the welded joints^[12].

Microhardness distribution of Ta and Mo side in the joint are shown in Fig. 7. The micro-hardness value of WZ is

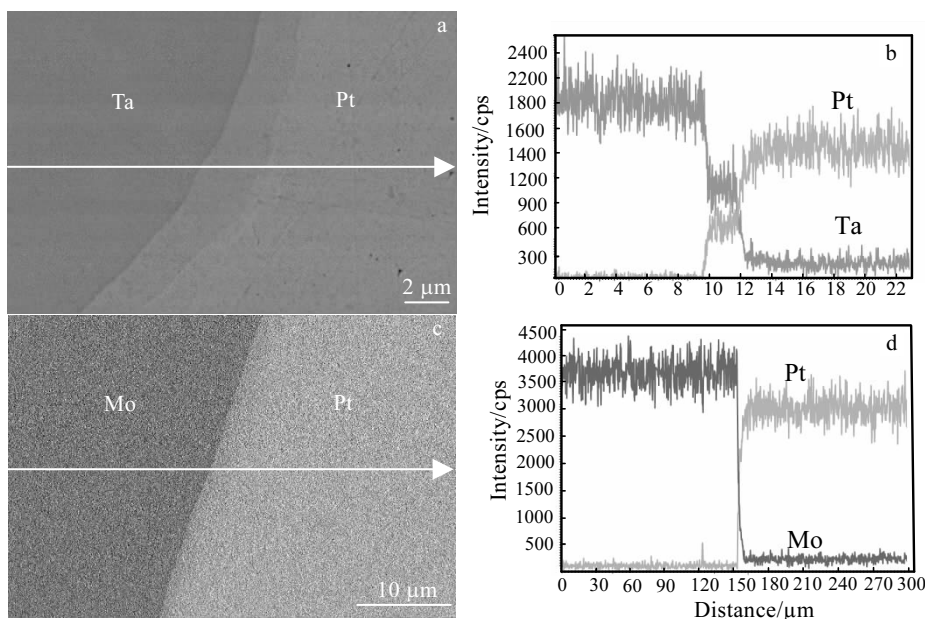


Fig. 4 Cross-sectional morphologies and the main element distribution of Ta/Mo joint: (a) Ta/Pt interface, (b) EDS linear scanning results of Fig.4a, (c) Mo/Pt interface, and (d) EDS linear scanning results of Fig.4c

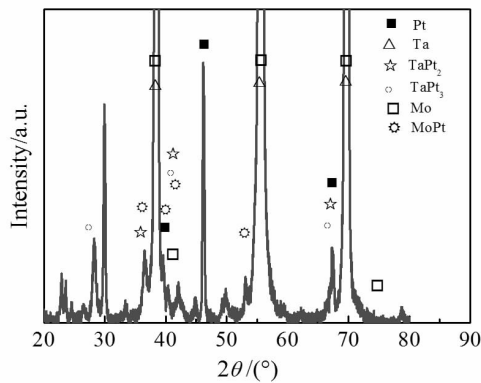


Fig.5 XRD pattern of the welding joint

much higher than that of BM. In the case of Ta side joint, a significant increase from the BM (1240 MPa) to WZ (1950 MPa) progressively. For the Mo side joint, a slight increase in micro-hardness of about 2100 MPa in BM to about 2400 MPa in the WZ and HAZ can be observed. The fluctuation of micro-hardness in the WZ is caused by the chemical inhomogeneity and uneven microstructures of welded joints. The higher hardness values were attributed to the formation of TaPt₂, TaPt₃ and MoPt phase. Similar extreme solid solution

strengthening was observed in Mo/Mo^[12], Ta/Mo^[2] and dissimilar joints^[13].

3 Discussion

3.1 Porosity defects

A small amount of porosities were observed in the WZ of welds in Fig.3 and Fig.4. The pores appeared when the most important laser parameter such as peak power of 1100 W or pulse duration of 4 ms was changed.

The origin of porosities most likely contain a mixture of entrapped air, Ar shielding gas, condensed metal vapor and changes in solubility of hydrogen during solidification^[2, 14-18].

Girard et al.^[19] studied the susceptibility of Ta to the formation of porosities in single spot welds during the solidification stage in the case of Ta joining. When the molten depth is less than 1.98 mm, the solidification time is less than 10 ms and the rise time is smaller than the minimum solidification time, the porosities can reach the melt surface and may be eliminated. This is a so called “no trapping region”. While no cracking or any other defects were found in the Ta/Ta joint with thickness of 0.2 mm, intergranular cracking occurred mainly along the centerline in the fuse zone of Mo/Mo joint (thickness 0.2 mm), as was reported by Zhou et al.^[2] For Huang et al. and Khan et al.^[17, 20] no

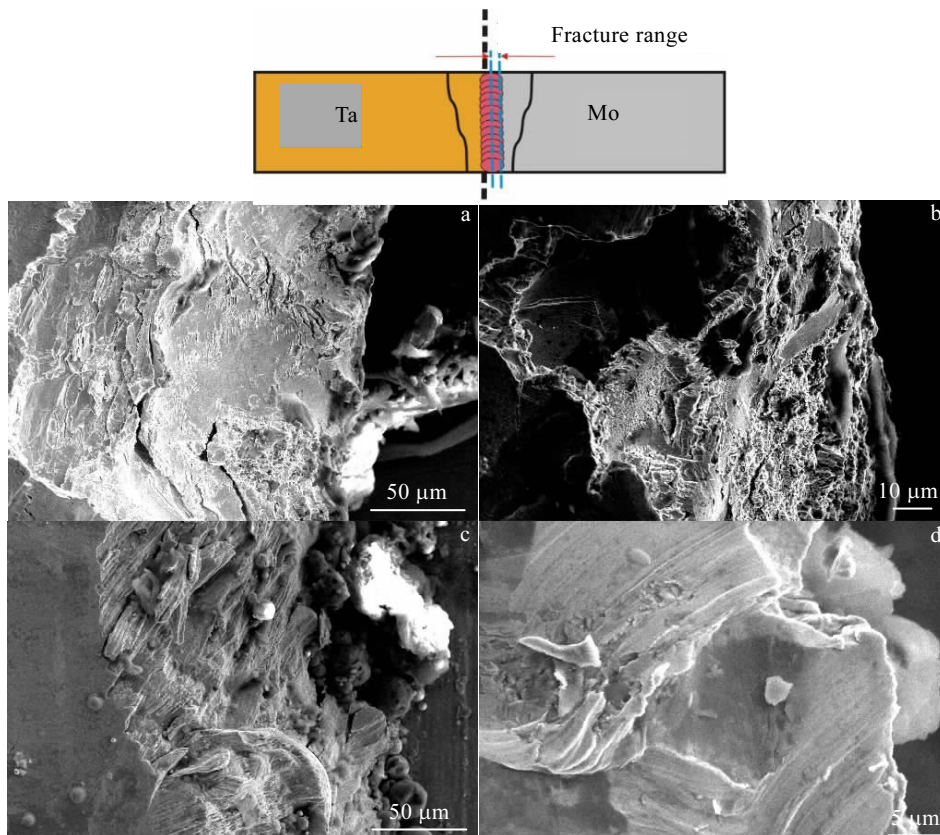


Fig.6 Fracture surface of Ta/Pt/Mo joint: (a) morphology of Ta side shear, (b) partial enlargement of Fig.6a, (c) morphology of Mo side shear, (d) partial enlargement of Fig.6c

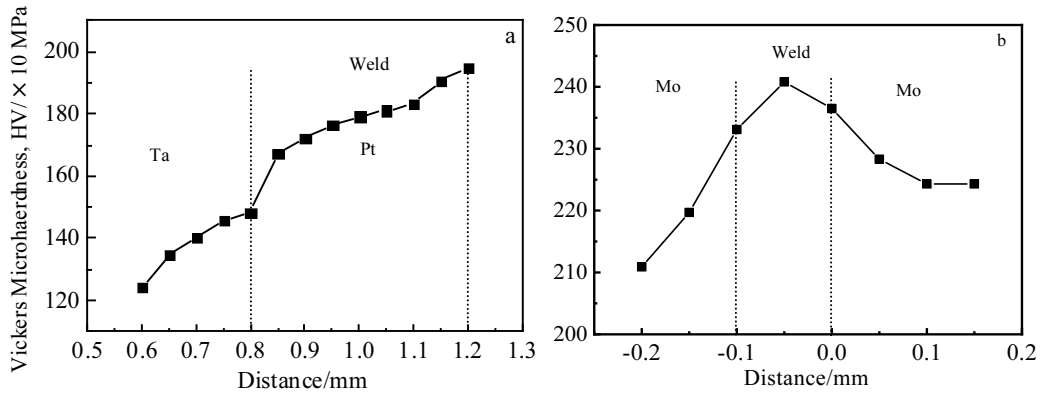


Fig.7 Microhardness distribution of Ta/Mo weld joint: (a) Ta side and (b) Mo side

porosity was observed when joining Pt-10 pct Ir wires to themselves. However, in this study, it was found that porosity occurs when joining the dissimilar materials together in the WZ of the joints. As the molten braze mixed with the molten Pt weld pool to create the WZ, the Pt element is preferentially vaporized due to relatively higher vapor pressures, promoting porosity. The alloying element vaporization during laser spot welding of stainless steel reported by He et al.^[21] and the low vaporization point element (Mg, Zn) content that tend to entrap occluded gases during welding by Haboudou et al.^[22] are examples of high vapor pressure metal elements. Furthermore, according to Collur et al., the mechanism of alloying element vaporization during laser welding was obtained by conducting isothermal experiments and the corresponding theoretically calculated values^[23]. The rate of vaporization of alloying elements during laser welding of stainless steels was controlled by plasma influenced intrinsic vaporization at the weld pool surface.

The primary driving force of vaporization is the total pressure gradient at the elevated temperatures experienced in the weld pool; therefore the likelihood for vaporization of elements in the WZ can be obtained using thermodynamic principles. The equilibrium vapour pressures (p_i^0) of the

various vaporizing elements, viz., Pt, Ta and Mo, over pure liquid were calculated using the following equations^[23-25].

$$\log_{10} p_i^0 = A + B/T + C \log_{10}(T) + DT + ET^2 \quad (1)$$

where p_i^0 is the equilibrium vapour pressures of element i over its pure liquid, T is temperature, A, B, C, D and E are the computing coefficients of element i .

The equilibrium vapor pressures of the elements in the WZ are plotted in Fig.8 with respect to temperature. Pt vapor pressure increases much faster with temperature compared to those of Ta and Mo. It indicates that Pt will preferentially vaporize in the pure liquid. A similar analysis was carried out by Huang et al.,^[18] on the porosity in Pt-Ir alloys. Furthermore, the Pt wire has a thermal diffusivity of 1.36 times that of Ta^[18,20], leading to higher freezing rates and less time for entrapped gasses to escape via buoyancy forces.

3.2 Electrical performance of electron guns

The support substrate of Mo and heat shield II of Ta are applied in the structure of electron gun, as shown in Fig.9. Mo is used to connect the cathode, while Ta is to prevent the thermal diffusion of heater assembly and support substrate of Mo. The function of each part plays an important role for the electron emission of electron gun.

In the development process of the microwave tubes, the main purpose of vacuum system for the electron gun is to obtain the data between current/voltage and temperature, to test the quick start parameter, to measure thermal expansion and to minimize the material evapotranspiration and outgassing. The performance of electron guns was tested in the ultra-high vacuum system, as shown in Fig.10. According to the structure and property of the electron gun, two operating station vacuum degassing system was designed and developed with the function of temperature measurement. The system final vacuum is better than 2×10^{-7} Pa. Mechanical pump is used as a backing up pump, while the molecular pump and the ion pump are the main pump. Each operating station can work independently or simultaneously to save time for increasing the efficiency in the production of electron guns. Indicator lights are equipped by the system to

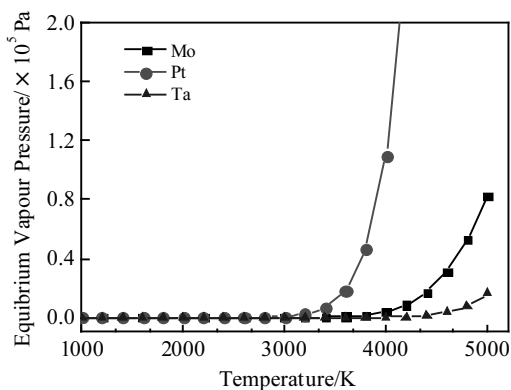


Fig.8 Calculated equilibrium vapour pressure of metal elements at different temperatures

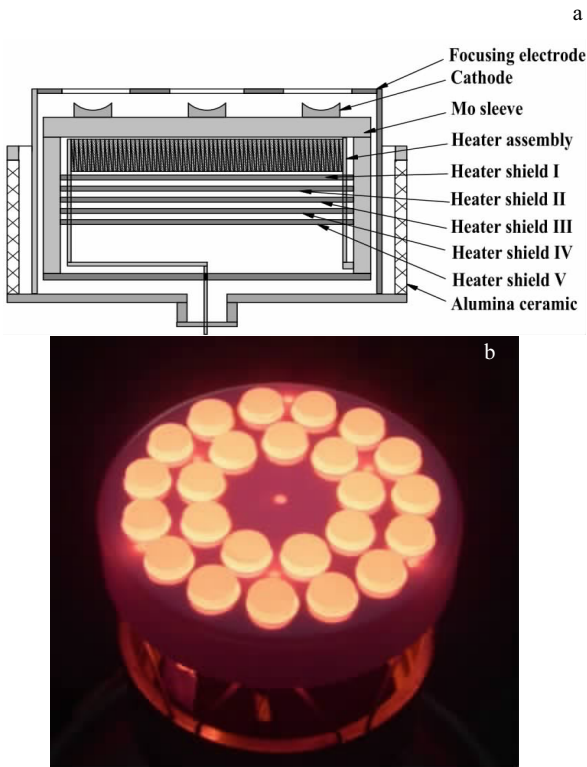


Fig.9 Structure chart of the electron gun

prevent the potential problems for the electron guns or the vacuum system that is caused by misoperation.

Fig.11 shows the curves among temperature, vacuum degree and current from three kinds of electron guns a, b and c. With the increase of the current, the cathode temperature increases significantly and when it increases from 5 A to 7 A the temperature changes from 855 °C to 1150 °C (see a₁ curve). At the same time, the vacuum degree decreases from 9×10⁻⁶ Pa to 5×10⁻⁵ Pa (see a₂ curve). Keeping the working current 7 A unchanged for a period of time, the cathode temperature tends to keep constant and the vacuum degree increases gradually. The reason may be that the material evapotranspiration from electron guns decreases gradually with increasing temperature. So it is the outgassing amount. The b and c electron guns show similar trends in temperature and vacuum degree.

According to the practical application, electron guns in the microwave tubes can be used at 1000 °C to 1300 °C for 3000~5000 h in the pulsed or continuous wave mode. High and low temperature thermal shock resistance of the welding components was studied and tested, with the property of long-period and high reliability. A large amount of data obtained from experiments verifies the working principal, structure design and good properties of electron guns. It is

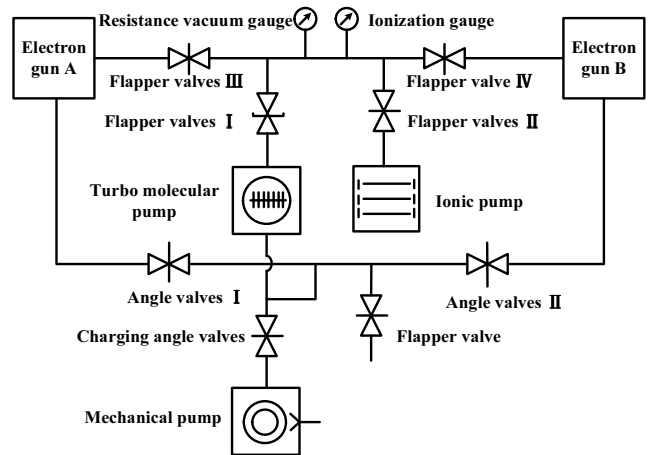


Fig.10 Ultra-high vacuum system for performance testing of electron guns

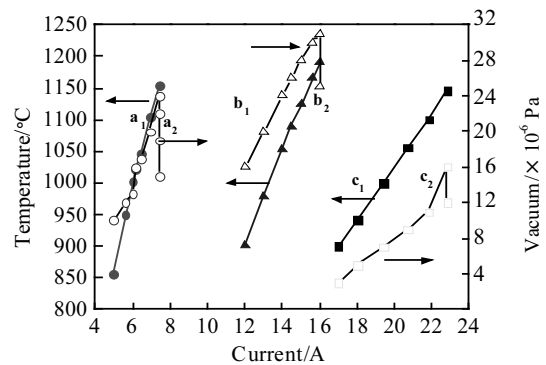


Fig.11 Curves among temperature, vacuum degree and current from three kinds of electron guns a, b and c: (a₁, b₁, c₁) current-temperature curves, (a₂, b₂, c₂) current-vacuum curves

applicable to different types of electron guns for microwave tubes, which is important significance in the small amount production of microwave tubes.

3.3 Environment adaptability

In order to adapt to the environment of random vibration and high shock, a design method of the support structure and welding process technology are introduced. Fig.12 shows the random vibration and high shock curves. It can be seen that all the experimental data lay on theoretical curves and the difference between practical and theoretical curves is very small. The structure of electron guns (see Fig.9) designed by this method can adapt the environment of random vibration and high shock well after the random vibration 5~500 kHz for 1 h and 10 g shock for 3 ms. Therefore, the welding joint is firm welding spot to meet the demands of design and process engineering.

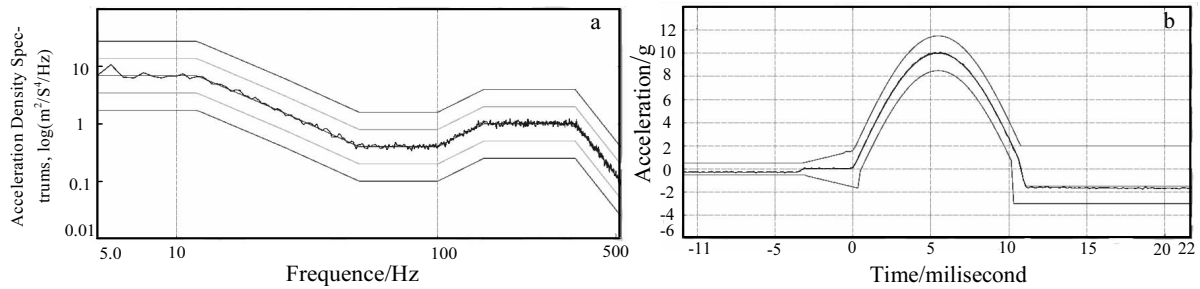


Fig.12 Random vibration (a) and high shock (b) curves

4 Conclusions

1) Ta/Mo dissimilar joint was successfully joined by laser welding process with pure Pt filler metal. The addition of Pt could achieve atomic diffusion or dissolution of the Pt element.

2) Output power and pulse duration are the most important parameters in defining the laser weld. The optimized laser parameters were: the output power is 1100 W, the pulse width is 4 ms, the pulse frequency is 3 Hz, the defocus distance is +1 mm and the Argon shielding gas is 10 L/min.

3) Due to the formation of Ta–Pt reaction layers at the weld zone/Ta interface, metallurgical bonding was achieved between Ta and Pt. TaPt_2 and TaPt_3 phase formed at the interface, corresponding to reaction product of laser weld. Mo and Pt elements have mutual diffusion and therefore, the MoPt phase formed at the interface between Mo and Pt weld zone.

4) The joint fracture initiated in the WZ and propagated to the HAZ and BM the fracture surface. The fracture surface of Ta/Mo joint exhibited typical brittle fracture characteristics. Brittle TaPt_2 , TaPt_3 and MoPt phase result in higher hardness in the WZ than that of the BM.

5) Pores in the weld was attributed to the preferential vaporization of pure Pt filler metal in the WZ, due to relatively higher vapor pressures than that of Ta and Mo.

6) Electrical performance, random vibration and high shock tests were performed to verify the welded joint equality and the property of electron guns with character of long-period and high reliability.

References

- Ding Yaogen. *Design, Manufacture and Application of High Power Klystron*[M]. Beijing: National Defense Industry Press, 2010
- Zhou X W, Huang Y D, Hao K et al. *Optics and Laser Technology*[J], 2018, 102: 54
- Wadsworth J, Morse G R, Chewey P M. *Materials Science and Engineering*[J], 1983, 59(2): 257
- Morito F. *Surface and Interface Analysis*[J], 1990, 15(7): 427
- Tabernig B, Reheis N. *Int Journal of Refractory Metals and Hard Materials*[J], 2010, 28: 728
- Zhang L J, Lu G F, Ning J et al. *Materials*[J], 2018, 11: 1852
- Hossick-Schott J, Reiterer M, Heffelfinger J et al. *The Journal of The Minerals, Metals & Materials Society*[J], 2003, 65: 625
- Nishio K, Masumoto H, Matsuda H et al. *Quarterly Journal of the Japan Welding Society*[J], 2003, 21: 302
- Pineau S, Veyrac M, Hourcade M et al. *Journal of the Less Common Metals*[J], 1985, 109: 169
- Grevey D, Vignal V, Bendaoud I et al. *Materials and Design*[J], 2015, 87: 974
- Zang C W, Liu J G, Tan C W. *Journal of Manufacturing Processes*[J], 2018, 32: 595
- Chen G Q, Liu J P, Shu X et al. *Vacuum*[J], 2018, 154: 1
- Cai X L, Sun D Q, Li H M et al. *Optics and Laser Technology*[J], 2017, 97: 242
- Zou G S, Huang Y D, Pequegnat A et al. *Metallurgical and Materials Transactions A*[J], 2012, 43A: 1223
- Huang Y D, Pequegnat A, Feng J C et al. *Science and Technology of Welding and Joining*[J], 2011, 16(7): 648
- Huang Y D, Lin X, Pequegnat A et al. *Journal of Wuhan University of Technology, Mater Sci Ed*[J], 2015, 30: 1286
- Huang Y D, Pequegnat A, Zou G S et al. *Metallurgical and Materials Transactions A*[J], 2012, 43A: 1234
- Huang Y D, He P, Lin T S et al. *Rare Metal Materials and Engineering*[J], 2013, 42(10): 2079 (in Chinese)
- Girard K, Jouvard J M, Naudy P. *Journal of Physics D-Applied Physics*[J], 2000, 33(21): 2815
- Khan M I, Kim J M, Kuntz M L et al. *Metallurgical and materials transactions A*[J], 2009, 40: 910
- He X, DebRoy T, Fuerschbach P W. *Journal of Physics D: Applied Physics*[J], 2003, 36: 3079
- Haboudou A, Peyre P, Vannes A B et al. *Materials Science and Engineering*[J], 2003, A363: 40
- Collur M M, Paul A, Debroy T. *Metallurgical Transactions B*[J], 1987, 18B: 733
- Yaws C L. *1994 Handbook of Vapor Pressure, Vol 4*[M]. Houston TX: Gulf Publishing Co, 1995
- Block-bolten A, Eagar T W. *Metallurgical Transactions B*[J], 1984, 15: 461

电子枪零件钽钼激光焊接显微结构和性能分析

王博锋^{1,2}, 胡旭华¹, 周冠丽¹, 周健勇¹, 张永清¹, 张兆传¹

(1. 中国科学院电子学研究所 中国科学院高功率微波源与技术国防科技创新重点实验室, 北京 100190)

(2. 中国科学院大学, 北京 100149)

摘要: 采用脉冲固体激光器对电子枪零件钽和钼进行激光焊接工艺试验, 利用金相显微镜、扫描电镜、万能材料试验机、电子显微硬度分析仪、X射线衍射仪、振动台、电子枪真空除气系统等研究了电子枪金属零件焊缝焊接表面成形、接头区域的组织形貌、界面元素分布、断口形貌、显微硬度与接头力学性能、焊接接头物相、电子枪振动冲击性能及工作状态下电性能和热性能。结果表明, 优化焊接参数后焊接的电子枪经受了在微波管中连续高温工作的考验。振动冲击试验和电子枪性能试验检验了电子枪组件的焊接牢固程度和焊接质量, 验证了激光焊接工艺在小批量微波管研制、生产和应用过程中的可靠性。

关键词: 钽; 钼; 钨; 激光焊接; 显微结构; 性能

作者简介: 王博锋, 男, 1988年生, 博士, 助理研究员, 中国科学院电子学研究所, 北京 101190, 电话: 010-56535231, E-mail: bfwang@mail.ie.ac.cn